# LEADING-EDGE VORTEX FLAPS FOR SUPERSONIC TRANSPORT CONFIGURATION -EFFECTS OF FLAP CONFIGURATIONS AND ROUNDED LEADING-EDGES-

**Kenichi RINOIE*, Dong Youn KWAK**, Katsuhiro MIYATA* and Masayoshi NOGUCHI****
***Department of Aeronautics and Astronautics, University of Tokyo, Tokyo, 113-8656, JAPAN**
****National Aerospace Laboratory, Tokyo, 181-0015, JAPAN**

**Keywords**: *vortex flap, rounded leading-edge, SST*

## Abstract

*Wind tunnel measurements were done on a cranked arrow wing SST configuration with leading-edge vortex flaps. Force and surface pressure measurements were made at the Reynolds number based on the wing mean aerodynamic chord of $9.2x10^5$ to $3.8x10^6$. Two different flap cross sections (the originally designed "non-rounded" leading-edge and the rounded leading-edge) were tested. The purpose of the measurements is to clarify how the differences of the Reynolds number affect the flow around the rounded leading-edge vortex flaps and the flap performance. The wing with the rounded leading-edge vortex flaps indicated some benefit of the lift/drag ratio as compared with those of the "non-rounded" vortex flaps at a relatively high lift coefficient greater than 0.3. Different flow patterns were observed over the rounded leading-edge vortex flaps when the Reynolds number is increased at a lift coefficient greater than 0.5. The spanwise length of the separated region shortens as the Reynolds number is increased. However, this flow pattern change has only a little influence on the wing lift/drag ratio itself in the range of the tested Reynolds numbers.*

## Nomenclature

| | |
|---|---|
| $b$ | local span, m |
| $b_{max}$ | wing maximum span length, m |
| $C_A$ | axial force coefficient |
| $C_D$ | drag coefficient |
| $C_L$ | lift coefficient |
| $C_m$ | pitching moment coefficient non-dimensionalized using $C_{mac}$ and measured about 0.25 $C_{mac}$ |
| $C_{mac}$ | wing mean aerodynamic chord, m |
| $Cp$ | pressure coefficient |
| $Cr$ | wing root chord at model center-line, m |
| $D$ | rounded leading-edge diameter, m |
| $L/D$ | lift/drag ratio |
| $M$ | free stream Mach number |
| $Re$ | Reynolds number based on mean aerodynamic chord |
| $U_\infty$ | free stream velocity, m/s |
| $x$ | chordwise coordinate measured from apex of delta wing at model centre-line, m |
| $y$ | spanwise coordinate orthogonal to $x$, measured from model centre-line, m |
| $\alpha$ | wing angle of attack, deg |
| $\delta_{fLEin}$ | inboard vortex flap deflection angle, deg |
| $\delta_{fLEout}$ | outboard leading-edge flap deflection angle, deg |

## 1 Introduction

A leading-edge vortex flap is a full span deflectable surface at the leading-edge of a delta wing [1]. With the flap deflected downward, a leading-edge separation vortex is formed over the forward facing flap surface. The suction force generated by the vortex acts on the flap and generates a thrust component. Hence, it reduces the drag and improves the lift/drag

(*L/D*) ratio, which is an essential factor for the improvement of the take-off and climb performance of the delta wing aircraft such as a next generation supersonic transport. Many studies have confirmed the benefit of the vortex flap [2-4].

The first author has made several experimental studies of vortex flaps for delta wing configurations [5-8]. These studies discussed the four main factors that affect the vortex flap characteristics: flap deflection angles [5], wing sweepback angles [6], leading-edge cross sections [7] and flap hinge-line positions [8]. Throughout these studies, the effects of these four factors were discussed.

It is known for a plain delta wing with rounded leading-edges that a large fraction of the leading-edge suction force acts on the rounded leading-edge and reduces the drag component of the delta wing [9-12]. Reference 7 shows a combination of the vortex flaps and the rounded leading-edge. By deflecting the rounded leading-edge vortex flaps, suction forces, which are caused both by the leading-edge separation vortex over the flap surface and by the rounded leading-edge, reduced the drag component and increased the lift/drag ratio. It was revealed in reference 7 that the 60° delta wing with the rounded-edged vortex flaps is more effective than the wing with sharp-edged vortex flaps when $C_L$ is relatively high ($C_L$ > 0.4).

In this paper, further studies have been conducted to clarify how the rounded leading-edge vortex flap improves the wing performance. The wing model tested has a cranked arrow wing that is used for a supersonic transport configuration. The vortex flap benefit on the supersonic transport configuration has been studied in references 13-15. In these studies, the leading-edge of the original wing, that was optimized for a supersonic cruise, was simply deflected as the vortex flap or a sharp-edged thin flat plate was attached on the lower surface of the wing as the vortex flap, while no references tested the effect of the flap cross section.

The wing configuration studied here is based on the cranked arrow wing configuration that was designed for a supersonic flight test programme currently underway by the National Aerospace Laboratory, Japan [16]. The original designed cranked arrow wing was modified so that the leading-edges can be deflected as leading-edge flaps. Two different leading-edge cross sections were tested, i.e., the original design (relatively sharp leading-edge) and the rounded leading edge that has a diameter of 2% of the wing mean aerodynamic chord.

It has been pointed out that the performance of a rounded-edged delta wing is affected by the Reynolds number [11]. In reference 7, tests were mainly conducted at a fixed single Reynolds number. In this paper, however, tests are conducted at several different Reynolds numbers to reveal the Reynolds number effect on the rounded leading-edge vortex flaps.

Here, a 2m x 2m low speed wind tunnel and a 2m x 2m transonic wind tunnel were used for the tests. The force and surface pressure measurements were made on this SST configuration model with different flap deflection angles and with different leading-edges. Measurements at the 2m x 2m low speed wind tunnel were made in a range of angles of attack at -4° to +30° at a Reynolds number based on the mean aerodynamic chord $C_{mac}$ of $9.2 \times 10^5$. The performance of the vortex flap with the original leading-edge has been investigated at this wind tunnel. Measurements at the 2m x 2m transonic wind tunnel were made in a range of angles of attack at -3° to +16° at the Reynolds numbers between $1.5 \times 10^6$ and $3.8 \times 10^6$ at a free stream Mach number $M$=0.3. The benefit of the rounded leading-edge vortex flaps and the effect of the Reynolds number on the rounded-edged vortex flaps were investigated in this wind tunnel.

In summary, the purpose of this study is to discuss the effect of the rounded leading-edge vortex flap for the SST configuration and to reveal the Reynolds number effect upon the rounded leading-edge vortex flaps.

## 2 Experimental Details

Figure 1 shows the model details. This SST configuration model is based on the cranked arrow wing configuration with a fuselage section that was preliminary designed for the supersonic flight test programme conducted by the National Aerospace Laboratory. It has a sweepback angle of 66° at the inboard section and 42° at the outboard section. The kink is located between the inboard and outboard wings at $y/(b/2)$=0.55. The main wing was designed based on the supersonic lifting surface theory [17] at a design Mach number of 1.7, so that the wing has a warped wing section. The inboard wing has a thickness distribution of a NACA 66-series aerofoil section with an average thickness chord ratio of 3%. The outboard wing has a biconvex aerofoil section with a maximum thickness chord ratio of 3%. Details of the wing cross section are shown in Figure 2 [18]. The leading-edge of this model was modified so that it has the vortex flaps on the inboard wing and the leading-edge flaps on the outboard wing (Fig.1). Since the sweepback angle of the inboard wing is large, the inboard leading-edge flap has been thought to act as the vortex flaps. The chord length of this inboard vortex flap is $0.1C_{mac}$. The chord length of the outboard leading-edge flap is 20% of the local chord length at each spanwise station. The vortex flap deflection angle $\delta_{fLEin}$ for the inboard wing is defined as the angle measured in the plane that is normal to the hinge line. The leading-edge flap deflection angle $\delta_{fLEout}$ for the outboard wing is defined as the angle measured parallel to the free stream. The tested flap deflection angles are $\delta_{fLEin}$=0°, 15°, 30° and $\delta_{fLEout}$=0°, 5°, 12.2°. The flaps have been designed so that there is no gap between the inboard leading-edge flap and the outboard leading-edge flap at the kink when ($\delta_{fLEin}$, $\delta_{fLEout}$)=(15°, 5°) and (30°, 12.2°). Two rows of pressure tappings are located on the upper surface ($x/Cr$=0.55 and 0.83). The nose section of the fuselage, that is 25% of the total fuselage length, is an ogive-cone-cylinder.

Rounded leading-edge flap configurations were tested by modifying the lower surface of the leading-edge of the inboard section of the original wing (Figure 3). The flap deflection angle is the same as the original flap section $\delta_{fLEin}$=0°, 15° and 30°. It has a constant leading-edge diameter $D$ of 0.01m (=$0.02C_{mac}$) between $y/(b_{max}/2)$= 0.21 and 0.46. The diameter is defined in the plane that is normal to the leading-edge line (see section A-A in Figure 1). This diameter decreases linearly from $y/(b_{max}/2)$=0.21 towards $y/(b_{max}/2)$=0.12 and from $y/(b_{max}/2)$=0.46 towards $y/(b_{max}/2)$=0.55, so that the leading-edge configurations at $y/(b_{max}/2)$=0.12 and 0.55 coincide with the original wing design. Since the lower surface of the original wing was modified to have a rounded leading-edge section, a true flap deflection angle is greater than $\delta_{fLEin}$ as can be seen in Figure 3. Even when $\delta_{fLEin}$=0° for the rounded leading-edge, the true flap deflection angle is about 12°. One additional pressure tapping is located at the leading-edge of the rounded leading-edge section at $x/Cr$=0.55 (Figure 3).

The experiments were made in a 2m x 2m low-speed wind tunnel and a 2m x 2m transonic wind tunnel at the National Aerospace Laboratory, Japan. At the 2m x 2m low speed wind tunnel, tests were made at a tunnel speed of $U_\infty$=30m/s. The Reynolds number based on the mean aerodynamic chord ($C_{mac}$ =0.46m) was $Re$=9.21x$10^5$. The freestream turbulence intensity of the tunnel is about 0.06%. The angle of attack was in a range from -4° to +30°. Lift, drag, and the pitching moment were measured using a six-component internal balance. Surface pressure distributions were measured using electronic scanning pressure sensors (ESP). All of the aerodynamic coefficients were calculated based on the original wing area without any flap deflection. The effects of the Reynolds number were tested at the 2m x 2m transonic wind tunnel using the same model. Tests were made at a tunnel speed of $M$=0.3. By altering the wind tunnel's total pressure, tests at different Reynolds numbers have been conducted. Five different Reynolds numbers were tested ($Re$=1.44 x $10^6$ - 3.83 x $10^6$). The root mean square value of the pressure fluctuation in the tunnel is less than 1.1% when normalized by the

free stream dynamic pressure. The angle of attack was in a range from -3° to +16°. Lift, drag, and the pitching moment were measured using a six-component internal balance. Surface pressure distributions were measured using a "Scanivalve". The estimated overall accuracy of the aerodynamic coefficients is ±1% at 20:1 odds. The estimated overall accuracy of the pressure coefficient is ±2% at 20:1 odds.

Examples of the notation used in this paper are as follows. S301200 is the original wing with $\delta_{fLEin}$=30° and $\delta_{fLEout}$=12°. R150500 is the rounded leading-edge with a flap deflection of $\delta_{fLEin}$=15° and $\delta_{fLEout}$=5°. The last two digits of this notation are reserved for the trailing-edge flap. The effects of the trailing-edge flap were also investigated using the same model and the results are described in [18].

## 3 Results and Discussion

### 3.1 Flap Performance of Original Wing

In this section, the performance of the original wing with flap deflection is briefly discussed. Figures 4a-4d show the lift, drag, pitching moment and lift/drag curves at $Re$=9.21x10$^5$. These figures show the results for the original SST configuration with no flap deflection (S000000), the configuration of the inboard vortex flap deflection $\delta_{fLEin}$=15° (S150000), that of the outboard leading-edge flap deflection $\delta_{fLEout}$=5° (S000500), and finally for the combinations of the vortex flap $\delta_{fLEin}$=15° and the leading-edge flap deflections $\delta_{fLEout}$=5° (S150500).

The $C_L$ vs. α curves in Fig.4a show that the vortex flap and leading-edge flap deflections (S150000, S000500 and S150500) slightly decrease $C_L$ as compared with S000000, especially when α is greater than 10°. The $C_D$ vs. α curves in Fig.4b show that $C_D$ decreases as compared with S000000 when the vortex flap and the leading-edge flap are deflected. The $C_m$ vs. $C_L$ curves in Fig.4c show that $C_m$ is slightly affected by the flap deflection except when S000500. References 5-8 indicated that the vortex flap has little effect on $C_m$ for the delta wings. The plan shapes of the wing and the flaps are different between the present cranked arrow configuration and the delta wings in [5-8]. This may be the reason for the different behaviour of $C_m$.

Figure 4d shows the lift to drag ratio ($L/D$) versus $C_L$. This figure shows that the vortex flap deflection (S150000) has only a little benefit when $C_L$ =0.2-0.6 as compared with that of S000000. The results of the outboard leading-edge flap (S000500) indicate that the $L/D$ is slightly improved for S000500 between $C_L$ =0.15 and 0.6. The maximum value of $L/D$ is also improved as compared with that of S000000. However, these results are not so encouraging as compared with those of the delta wing with the vortex flaps reported in references 5-8.

When the vortex flaps and the leading-edge flaps are deflected at the same time (S150500), a higher benefit can be seen in the $C_L$ range of 0.2 and 0.7. The % increase in $L/D$ for S150500 as compared with the S000000 is about 12% between $C_L$=0.25 and 0.5. It has been reported in [15] that the $C_L$ range at SST's take-off is between 0.4 and 0.6. In this paper, the results at $C_L$=0.4-0.5 will be referred to as a reference that indicates the flap performance. The combined use of the vortex flaps and the leading-edge flaps shows some benefit for the performance of the SST configuration.

Figure 5 shows the surface pressure distributions for the same four different flap configurations as in Fig.4, in the spanwise direction for the upper surface at $x/Cr$=0.55 and 0.83 when α=5° and 10°. Fig.5a indicates that the vortex flap (S150000) suppresses the separation over the flap surface at a relatively low angle of attack (α=5°) at $x/Cr$=0.55. This agrees with the observation reported in [5]. Figure 5b (α=10°, at $C_L$≅0.4) indicates that as for S150000, the spanwise length of the separated region at $x/Cr$=0.55 (upper part of the figure) is reduced as compared with S000000 and the location of this separated region is confined mainly on the vortex flap surface. This confirms the description made in section 2 that the inboard flap deflection (S150000) works as the vortex flap, and thus the $L/D$ has slightly

been improved at $C_L \cong 0.4$ as was discussed in Fig.4d.

As for the outboard leading-edge flap configuration (S000500), Fig.5a ($\alpha$=5°, $C_L \cong 0.2$) shows that the separation is suppressed at $x/Cr$=0.83 (lower part of the figure). This suppression may have improved the $L/D$ at $C_L \cong 0.2$ as was discussed in Fig.4d. Figure 5b ($\alpha$=10°, at $C_L \cong 0.4$) indicates that as for S000500 there are two suction peaks at $x/Cr$=0.83. The first suction observed on the flap surface is caused by the separation at the leading-edge of the outer leading-edge flap. The second suction peak is observed near the kink station ($y/(b/2)$=50-70%). Since the suction peak near the kink is also observed on S000000 in this figure, this suction is thought to be caused by the separation from the kink or the inboard wing section.

When the inboard vortex flaps and the outboard leading-edge flaps are deflected at the same time (S150500), Figs.5a and 5b show that at $x/Cr$=0.55 the pressure distribution of this configuration is quite similar to that of S150000. This means that S150500 is working as the vortex flap at $x/Cr$=0.55 when $\alpha$=10°. At $x/Cr$=0.83, the $Cp$ distributions indicate that the S150500 behaves like S150000 at the inboard section near $y/(b/2)$=50-70% (please note that the suction region near the kink at $\alpha$=10° is not observed that was seen in S000500) and this may have helped to reduce the drag. Because of these reasons, the combination of the inboard vortex flaps and the outboard leading-edge flaps improves the $L/D$ as was seen in Fig.4d.

Tests at $\delta_{fLEin}$=30° and $\delta_{fLEout}$=12.2° were also conducted. The results of S301200 indicated similar characteristics to those of S150500.

## 3.2 Effects of Rounded Leading-edge

Figure 6 shows the lift, drag, pitching moment and lift/drag curves when the wing has an inboard rounded leading-edge with and without flap deflection (R000000 and R150500) together with the results from the original wing (S000000 and S150500) at $Re$=3.41x10$^6$. When the inboard vortex flap was deflected 15°, the outboard leading-edge flap was also deflected 5° to minimize the gap between these flaps. The lift to drag ratio ($L/D$) vs. the $C_L$ curve indicates that R000000 shows better $L/D$ ratios than does S000000 when $C_L$ values are greater than 0.2. A suction effect of the rounded leading-edge is demonstrated. The rounded leading-edge vortex flaps (R150500) also indicate better $L/D$ ratios when compared with those of S150500 when $C_L$>0.3. The % increase in $L/D$ for R150500 as compared with S000000 is about 27% at $C_L$=0.4 at this Reynolds number. These results conform the benefit of the rounded leading-edge vortex flaps as in [7].

Figure 7 shows surface pressure distributions at $x/Cr$=0.55 for these four configurations at $\alpha$=8°, 10° and 12°. The formation of the leading-edge separation vortex is observed for most of the configurations. These figures indicate that as the leading-edge radius is increased (S000000 → R000000 and S150500 → R150500), the spanwise length of the suction region is reduced. A similar trend was seen in [7].

Experiments with a 30° inboard vortex flap deflection (R301200) were also conducted. However, nothing beneficial was observed as compared with those of S301200. This may be explained by the drag increase due to the flow separation occurring underneath the flap because of a high deflection angle at the lower surface of the rounded-edged flap (Fig.3c).

### *3.2.1 Effects of Reynolds Numbers*

Figure 8 shows the $Cp$ distributions ($\alpha$=12°, 14° and 16° at $x/Cr$=0.55) when the Reynolds number is increased for the original (NACA 6-series "non-rounded") leading-edge wing with flap deflection (S150500). The $Cp$ distributions in this figure show only a small difference in the cases at different Reynolds numbers. This clearly indicates that the flow around S150500 is not affected by the Reynolds numbers.

Figures 9a and 9b show the $L/D$ and the axial force coefficient $C_A$ distributions at

different Reynolds numbers for the rounded leading-edge wing (R150500). $C_A$ is defined by

$$C_A = C_D \cos\alpha - C_L \sin\alpha$$

The negative value of $C_A$ is caused by the leading-edge suction force and by the suction pressure acting on the positive slope area on the upper rounded surface of the deflected flap. Although a high *L/D* benefit was expected as the Reynolds number is increased, the *L/D* distributions in Fig.9a show only a small increase in *L/D*. The $C_A$ distributions in Fig.9b also show that the $C_A$ is not so affected by the difference in the range of the tested Reynolds numbers. However, the *Cp* distributions in Fig.10 indicate that as the Reynolds number is increased, the suction peak decreases and the spanwise length of the suction region is reduced especially at $\alpha$=14° and 16°.

In order to clearly see the flow pattern changes when the Reynolds number is increased, cross flow patterns over the flap surface are plotted against $\alpha$ and *Re* in Figure 11 (S150500) and Figure 12 (R150500). Cross flow patterns are deduced from the surface pressure measurements at *x*/*C*r=0.55. The angles of attack $\alpha$, when the *L/D* attains its local maximum for a constant *Re* and when the $C_L$ equals about 0.5, are specifically indicated in these figures. Typical flow patterns and the examples of corresponding pressure distribution are also shown. Figure 11 shows that as for S150500 the flow in the cross flow planes at *x*/*C*r=0.55 can be divided into three different regimes. First, in regime (A) the leading-edge separation vortex is not formed or only a small separation bubble is formed at the leading-edge. Second, in regime (B) the leading-edge separation vortex is formed over the flap surface. Third, in regime (C) a large separation vortex is formed and its reattachment line is located inboard of the flap hinge line. Figure 11 also shows that the $\alpha$, where the boundary between these three regimes lies, are almost identical for different Reynolds numbers. This agrees with the discussion made in Fig.8, where the Reynolds number tested here does not affect the flow over S150500.

Figure 12 indicates the cross flow pattern distributions for R150500. Here, the flow is divided into four different regimes. Regimes A and C are the same as in Fig.11. However, regime B in this figure is divided into two (B-1 and B-2). Regime B-1 in Fig.12 corresponds to regime B in Fig.11. In regime B-2, the leading-edge separation vortex is formed on the flap surface as in regime B-1. However, inboard of the flap hinge line, the *Cp* distributions indicate that there is a small suction region. This may indicate that the flow separation occurs inboard of the flap hinge line. However, since the suction pressure is very small and the dominant flow pattern is the leading-edge separation vortex on the flap surface, we have named this region as B-2, a kind of the derivation from regime B-1. Figure 12 indicates that as the Reynolds number is increased, the $\alpha$ where the boundary between regime C and B-2 increases in the $\alpha$ axis when $Re>2.5\times10^6$. This corresponds to the flow observed in Fig.10 where the flow pattern changes as the Reynolds number is increased. The Reynolds number effect is observed at a higher *Re* and a higher $\alpha$ ($C_L>0.5$). However, as was seen in Fig.9, this flow pattern change has only a little influence on the wing lift/drag ratio itself in this test.

### *3.2.2 Effects of Surface Roughness*

It has been thought that the reason for the Reynolds number effects observed in the previous section is the difference of the boundary layer transition position over the flap surface. Therefore, supplementary tests were made at the 2m x 2m low speed wind tunnel ($Re=9.21\times10^5$) to examine the Reynolds number effect by adding roughness to the leading-edge of the upper surface of the model with a rounded leading-edge (R150500). The roughness used was an adhesive thin strip of 0.15mm thickness and 1mm width. These strips were attached at three different positions separately (No.1, 2 and 3), i.e., roughness No.1 was 4mm from the leading-edge, No.2 was 8mm and No.3 was 12mm (Figure 13). The strips located at the position of roughness No.1 would be sufficient to cause the transition to

turbulent flow, according to the estimation method based on [19] if the flow is a two dimensional one. The main focus of roughness was to see the sensitivity of the results to the Reynolds number by simulating the turbulent boundary layer that is expected at a higher Reynolds number.

Figure 13 shows the surface pressure distributions for R150500 at $\alpha$=14° and 16° with roughness No.1, No.2, No.3 and also without roughness. This indicates that as the roughness position moves towards the leading-edge (No.3 -> No.1), the spanwise length of the suction region becomes shorter. When compared with these data and those in Fig.10, it can be said that these two figures show quite similar distribution. This means that the effect of the Reynolds number may also have a strong relationship with the flow transition. This can explain part of the reason behind the difference in the extent and the strength of the separated region over the flap surface that was seen in Fig.12. Since the flow considered here is the one around the rounded leading-edge of a sweptback wing, it may be thought that the transition is affected by a cross flow instability.

It should be pointed out that the rounded leading-edge can only be used when flying at low speed, because of a high wave drag penalty at supersonic speeds. Therefore, a similar kind of Kruger flap, that can alter the wing leading-edge cross section into the rounded one, may be applied onto the lower surface of the wing, so that it works as the rounded-edged vortex flap when required.

## 4 Conclusions

Wind tunnel measurements were done on a cranked arrow wing SST configuration. Two different flap cross sections (originally designed NACA 6-series "non-rounded" leading-edge and the rounded leading-edge) were tested. The purpose of the measurements is to clarify how the differences of the Reynolds number affect the flow around the rounded leading-edge vortex flaps and the flap performance.

1) The combination of the "non-rounded" vortex flaps at the inboard wing and the leading-edge flaps at the outboard wing shows a lift/drag ratio benefit in the lift coefficient range of 0.2 to 0.7 as compared with the wing without flap deflections.

2) The rounded leading-edge vortex flaps indicate some benefit of the lift/drag ratio as compared with those of "non-rounded" vortex flaps at a relatively high lift coefficient greater than 0.3.

3) Different flow patterns were observed over the rounded leading-edge vortex flaps when the Reynolds number is increased at the lift coefficient greater than 0.5. At a lower Reynolds number, a separation vortex that has a relatively long spanwise length is formed. When the Reynolds number is increased, the spanwise length of the separated region shortens. However, this flow pattern change has only a little influence on the wing lift/drag ratio itself in this test.

## References

[1] Rao D M. Leading edge vortex-flap experiments on a 74deg. delta wing. NASA CR-159161, 1979.

[2] Marchman III J F. Effectiveness of leading-edge vortex flaps on 60 and 75 degree delta wings. *Journal of Aircraft*, Vol. 18, No. 4, pp 280-286, 1981.

[3] Frink N T. Subsonic wind-tunnel measurements of a slender wing-body configuration employing a vortex flap. NASA TM-89101, 1987.

[4] Levin D and Seigner A. Experimental investigation of vortex flaps on thick delta wings, *Journal of Aircraft*, Vol. 31, No.4, pp 988-991, 1994.

[5] Rinoie K and Stollery J L. Experimental studies of vortex flaps and vortex plates. *Journal of Aircraft*, Vol. 31, No. 2, pp 322-329, 1994.

[6] Rinoie K, Fujita T, Iwasaki A and Fujieda H. Experimental studies of a 70-degree delta wing with vortex flaps. *Journal of Aircraft*, Vol. 34, No. 5, pp 600-605, 1997.

[7] Rinoie K. Experiments of a 60-degree delta wing with rounded leading-edge vortex flaps. *Journal of Aircraft*, Vol.37, No.1, pp 37-44, 2000.

[8] Rinoie K and Kwak D Y. Studies on vortex flaps having different flap hinge-line positions, *Journal of Aircraft*, Vol.38, No.2, pp 396-398, 2001.

[9] Jones R, Miles J W and Pusey P S. Experiments in the compressed air tunnel on swept-back wings including two delta wings, A.R.C. R. & M. 2871, 1954.

[10] Fletcher H S. Low-speed experimental determination of the effects of leading-edge radius and profile

thickness on static and oscillatory lateral stability derivatives for a delta wing, NACA TN-4341, 1958.

[11] Henderson W P. Effects of wing leading-edge radius and Reynolds number on longitudinal aerodynamic characteristics of highly swept wing-body configurations at subsonic speeds, NACA TN D-8361, 1976.

[12] Chu J and Luckring M. Experimental surface pressure data obtained on 65° delta wing across Reynolds number and Mach number ranges, NASA TM 4645, 1996.

[13] Yip L and Murri D G. Effects of vortex flaps on the low-speed aerodynamic characteristics of an arrow wing, NASA TP 1914, 1981.

[14] Coe P L Jr, Kjelgaard S O and Gentry G L Jr. Low-speed aerodynamic characteristics of a highly swept, untwisted, uncambered arrow wing, NASA TP 2176, 1983.

[15] Nicholls K P. Flap systems on supersonic transport aircraft, Proc. CEAS European forum on high lift and separation control, Bath, U.K. pp 3.1-3.6, 1995.

[16] Sakata K. Supersonic experimental airplane programme and related activities in Japan, 23rd Congress ICAS, Toronto, Canada, ICAS-2002-1.6.1, 2002.

[17] Carlson H W and Miller D S. Numerical method for the design and analysis of wings at supersonic speeds, NASA TN D-7713, 1974.

[18] Kwak D Y, Miyata K, Noguchi M, Sunada Y and Rinoie K. Experimental investigation on high lift devices for an SST, Technical Report of National Aerospace Laboratory, to be published (in Japanese).

[19] Schlichting H. *Boundary-Layer Theory*, 7th ed., McGraw-Hill, New York, 1979, pp 538-542.

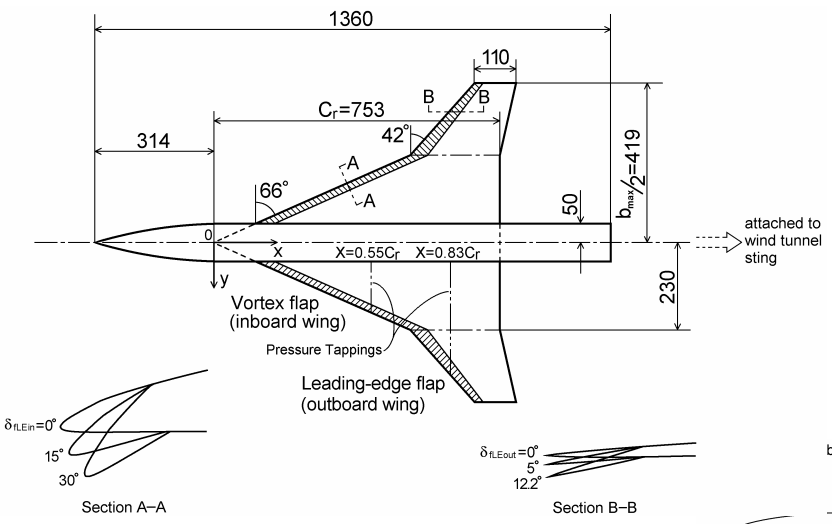


Fig.1 SST Model (unit: mm)

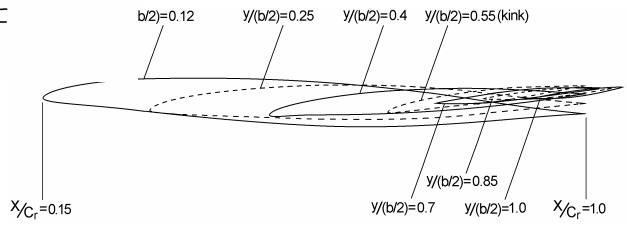


Fig.2 Cross Sections of Original Designed Wing (Vertical axis has been enlarged twice as long for clarity.)

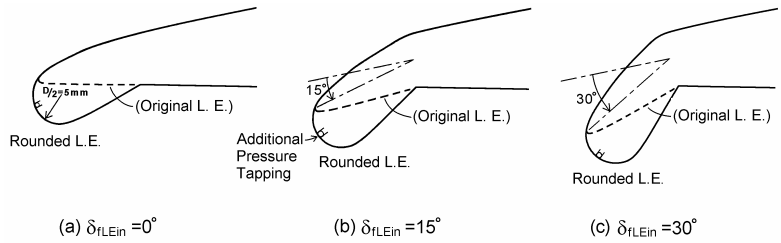


Fig.3 Rounded Leading-Edges (Section A-A in Fig.1)

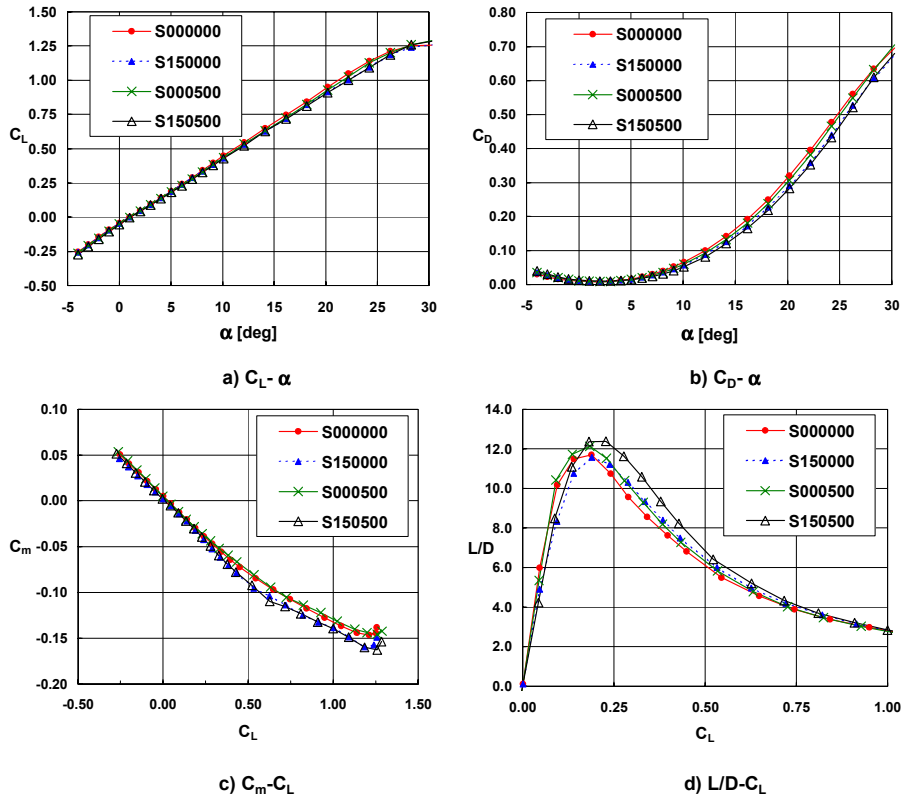


Fig.4 Effects of Vortex Flaps and Leading-Edge Flaps for Original Leading-Edge (Force Measurements, *Re*=9.21x10$^5$)

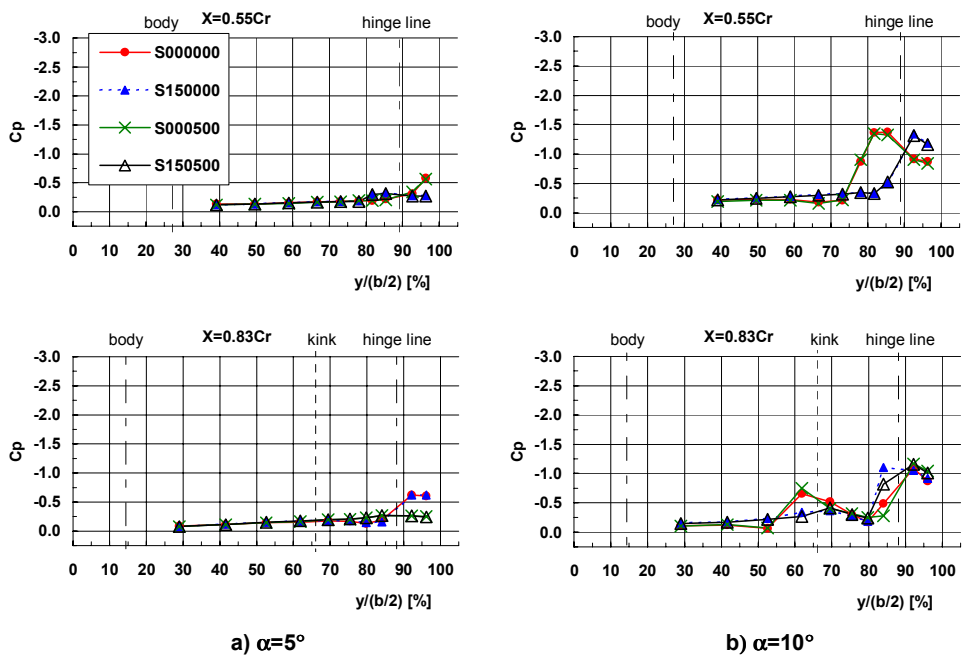


Fig.5 Effects of Vortex Flaps and Leading-Edge Flaps for Original Leading-Edge (Surface Pressure Measurements, *Re*=9.21x10$^5$)

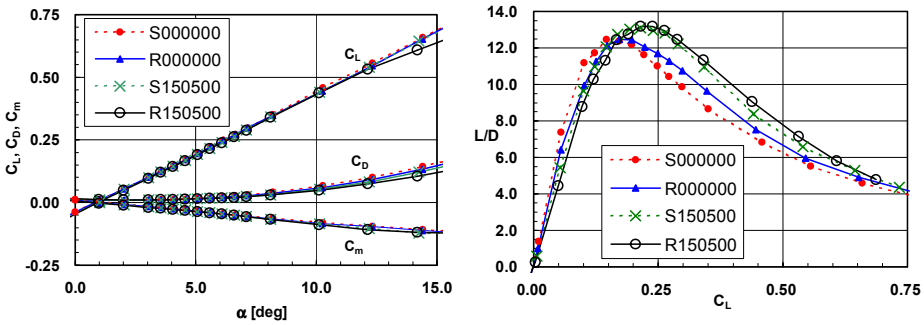


Fig.6 Effects of Rounded Leading-Edge with and without Flap Deflection (Force Measurements, $Re$=3.41x10$^6$)

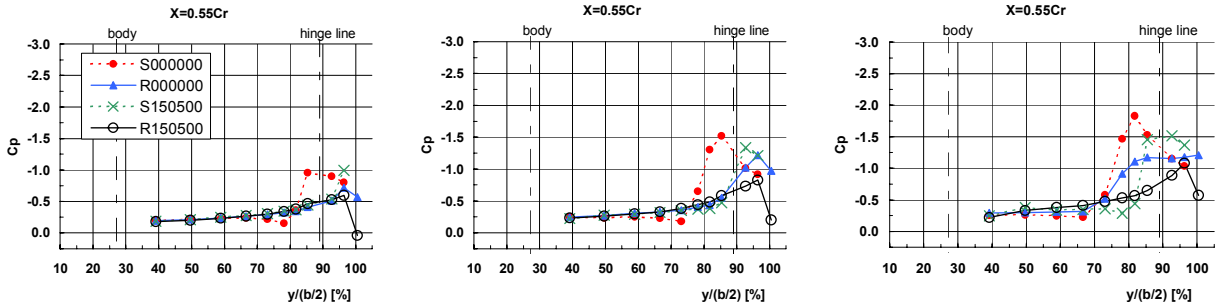


a) α=8° b) α=10° c) α=12°

Fig.7 Effects of Rounded Leading-Edge with and without Flap Deflection (Surface Pressure, $Re$=3.41x10$^6$)

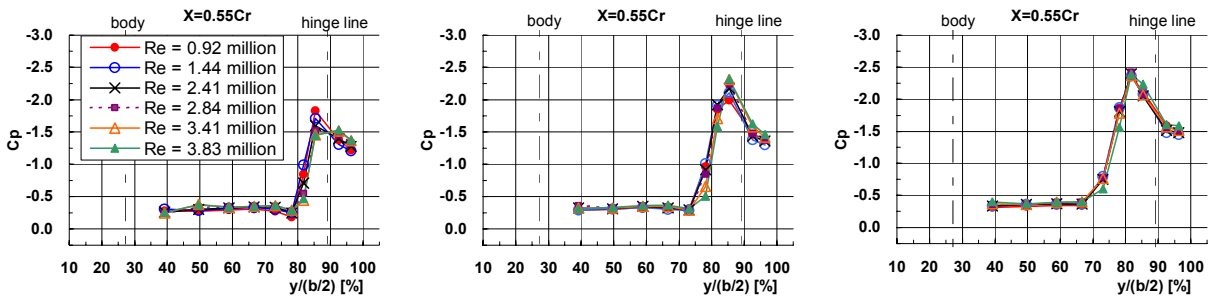


a) α=12° b) α=14° c) α=16°

Fig.8 Effects of Reynolds Number on Original Leading-Edge Wing (Surface Pressure, S150500)

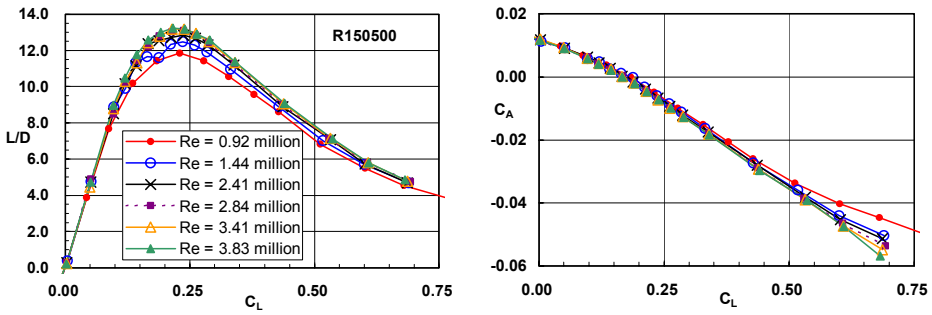


a) L/D - $C_L$ b) $C_A$ - $C_L$

Fig.9 Effects of Reynolds Number on Rounded Leading-Edge ($L/D$-$C_L$ and $C_A$-$C_L$, R150500)

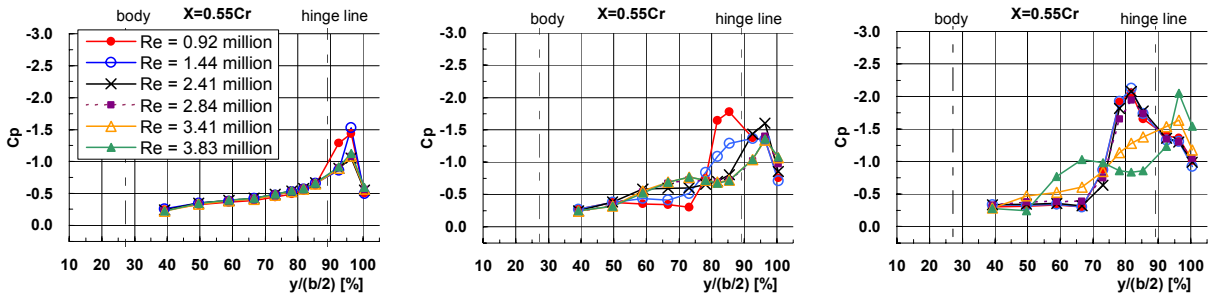


a) α=12° b) α=14° c) α=16°

Fig.10 Effects of Reynolds Number on Rounded Leading-Edge (Surface Pressure, R150500)

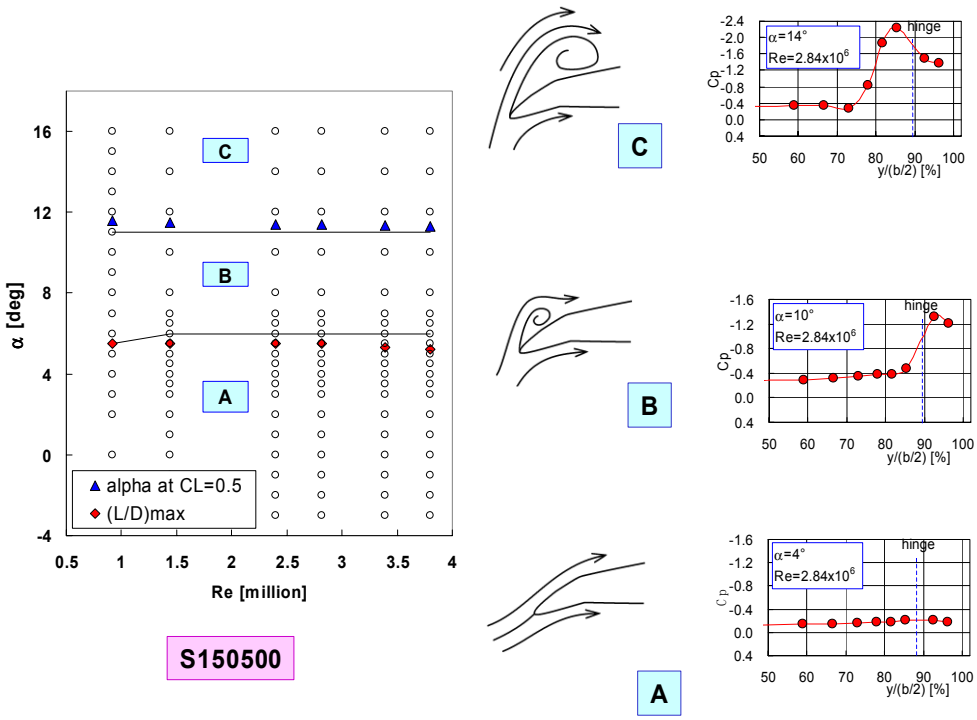


Fig.11 Crossflow Patterns at Different Reynolds Number for S150500

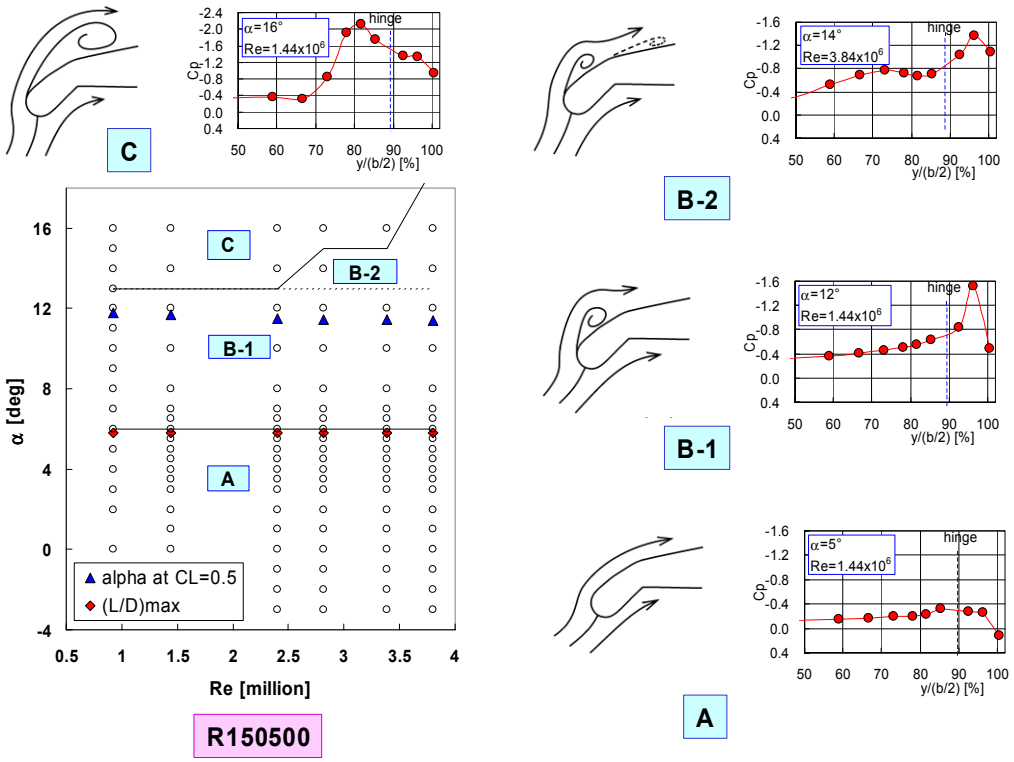


Fig.12 Crossflow Patterns at Different Reynolds Number for R150500

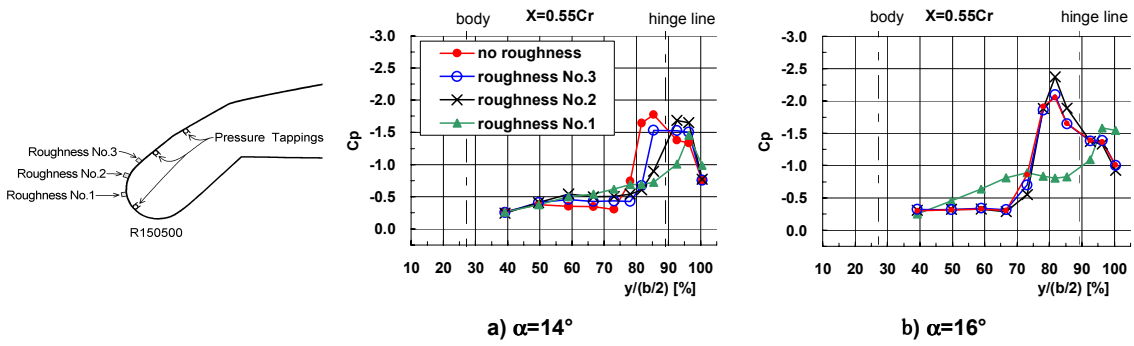


Fig.13 Effects of Surface Roughness (Surface Pressure, R150500, $Re$=9.21x10$^5$)